$[Cu_{58}(SeC_6H_5)_{24}(Dppe)_6Se_{16}]^{2+}$ Assembled from Tetrahedra and Octahedron: Synthesis, Characterization, Structure and Catalytic properties

Tao Yang,[a] Jianmei Jia,[a] ling Xiong,*[,b] Shan Jin,*[,a] and Manzhou Zhu[a]

a. Key Laboratory of Structure and Functional Regulation of Hybrid Materials, Anhui University, Ministry of Education, Institutes of Physical Science and Information Technology, Anhui University, Department of Chemistry and Center for Atomic Engineering of Advanced Materials, Anhui University, Anhui 230601, China

b. School of Food and Chemical Engineering, Shaoyang University, Shaoyang 422000, China

1.1 Chemicals Materials

Copper tetraacetonitrile tetrafluoroborate ($Cu(CH_3CN)_4 \cdot BF_4$), 98.3%, Sigma-Aldrich), diphenyl phosphine ethane (Dppe, 99.7%, Sigma-Aldrich), phenylselenol (C_6H_5SeH, 96 %, Sigma-Aldrich), tert-butylamine borane ($C_4H_{11}BN$, 98%, Sigma-Aldrich), acetonitrile (CH_3CN, HPLC, Aldrich), chloroform ($CHCl_3$, HPLC grade, Aldrich) n-hexane (Hex, HPLC grade, Aldrich), dichloromethane (CH_2Cl_2, HPLC grade, Aldrich). All reagents were used as received without further purification.

1.2 The synthesis of isomer Cu_{58} clusters

The synthesis of $[Cu_{58}(SePh)_{24}(Dppe)_6Se_{16}]^{2+}$ was successfully achieved under mild conditions using a one-pot method. Initially, 160 mg of $Cu(MeCN)_4BF_4$ was added to a reaction flask containing 5 ml of acetonitrile and 5 ml of chloroform. This mixture was left to stand for 5 minutes to ensure proper dissolution. Subsequently, 50 mg of Dppe (1,2-bis(diphenylphosphino)ethane) was introduced into the flask. Following this, 25 ul of PhSeH (phenylselenol) was added to the mixture, and the reaction was stirred for another 15 minutes to allow for adequate interaction and preliminary reaction of the PhSeH with the copper complex. After this period, 2 ml of methanol, in which 100 mg of tert-butylamine borane had been dissolved, was added to the mixture, leading to further reaction and nanocluster formation. Over the course of 4 hours, the reaction mixture gradually turned into a dark red solution, indicating the formation of the desired nanocluster.

The next step involved extracting the reaction mixture with CH_2Cl_2 to separate the product from the reaction solvents and byproducts. The organic phase was then washed with n-hexane to remove any remaining impurities. The purified solution was set up for crystallization. Single crystals suitable for X-ray analysis were obtained by allowing the solution to slowly evaporate under a controlled n-hexane/CH_2Cl_2 (3:1) vapor diffusion condition. After approximately 30 days, black cube-shaped crystals formed, confirming the successful synthesis of the desired nanocluster. The yield of $[Cu_{58}(SeC_6H_5)_{24}(Dppe)_6Se_{16}]^{2+}$(20 mg, 0.0018 mmol) was about 20.5% (Cu atom basis).

This detailed yet straightforward methodology exemplifies the effectiveness of the one-pot synthesis approach under mild reaction conditions, yielding high-quality single crystals of the nanocluster.

1.3 Characterization

All nanoclusters' UV/Vis absorption spectra are recorded using a METASH UV-8000PC. Electrospray ionization time-of-flight mass spectrometry (ESI-TOF-MS) measurement was performed using a UPLC H-class/XEV0G2-XS QTOF high-resolution mass spectrometer. The sample was directly infused into the chamber at 5 μL/min. X-ray photoelectron spectroscopy (XPS)

measurements were performed on a Thermo ESCALAB 250 configured with a mono chromated AlKα (1486.8 eV) 150W X-ray source, 0.5 mm circular spot size, a flood gun to counter charging effects, and the analysis chamber base pressure lower than 1 x 10^{-9} mbar, data were collected with FAT= 20 eV. Electrochemical experiments were performed on a CHI 660e. A platinum mesh was used as the working electrode. A Pt foil and Ag/AgCl served as the counter and reference electrodes, respectively. The concentration of the samples was ~0.015 mM with 0.1 M TBAP in10 ml CH_2Cl_2, and the solution was purged with argon for 10 min before experiments. All data were collected at room temperature.

1.4 X-Ray Crystallography

The data collection for single-crystal X-ray diffraction (SC-XRD) of all nanocluster crystal sampleswas carried out on Stoe Stadivari diffractometer under nitrogen flow, using graphitemonochromatized Cu Kα radiation (λ = 1.54186 Å). Data reductions and absorption corrections were performed using the SAINT and SADABS programs, respectively. The structure was solved by direct methods and refined with full-matrix least squares on F^2 using the SHELXTL software package. All non-hydrogen atoms were refined anisotropically, and all the hydrogen atoms were set in geometrically calculated positions and refined isotropically using a riding model.

1.5 Computational methods and details

The structure optimization of **Cu_{58}** is implemented in CP2K software [S1] based on density functional theory (DFT). The optimization process is carried out by Perdew-Burke-Erzerhof (PBE)/D3BJ method[S2,S3] with the combination of DZVP-MOLOPT-SR-GTH and GTH-PBE pseudopotential. The size of the box is set to 27.74338289*27.74338289*27.74338289 to ensure the precision and accuracy of structural optimization. The convergence limits of the maximum geometry change, RMS geometry change, maximum force and RMS force in geometric optimization are set to 3E-3, 1.5E-3, 4.5E-4 and 3E-4, respectively.

The single point energies of **Cu_{58}** was calculated using DFT at the PBE0-D3(BJ)[S4,S5]/def2-TZVP[S6] level, as implemented in the ORCA5.0.3 program system[S7,S8]. TDDFT calculation is implemented using the ORCA5.0.3 program system at the level of PBE0[S9]/def2-SV(P)[S6]. The number of excited states calculated for **Cu_{58}** cluster is 400.

In view of the size of the overall structure of **Cu_{58}**, we simplified all benzene rings to methyl groups in the above calculations to ensure the smooth implementation of these calculation tasks. In addition, the density-fitting approximation method is used to accelerate the calculation of single point energy and TDDFT (the error introduced is negligible). The density fitting basis set used is def2/J[S10] (corresponding to the def2-SV(P) and def2-TZVP basis set, respectively). The maps of UV-Vis, ECD and PDOS are all plotted based on the data analyzed by Multiwfn3.8(dev) software package[S11]. In addition, the three-dimensional contour maps of real space functions such as MOs, hole-electrons, C_{ele} and C_{hole} are all drawn using Multiwfn3.8(dev) combined with VMD software.

[S1] T. D. Kühne.; M. Iannuzzi.; M. D. Ben.; V. V. Rybkin.; P. Seewald.; F. Stein.; T. Laino.; R. Z. Khaliullin.; O. Schütt.; F. Schiffmann.; D. Golze.; J. Wilhelm.; S. Chulkov.; M. H. Bani-Hashemian.; V. Weber.; U. Borštnik.; M. Taillefumier.; A. S. Jakobovits.; A. Lazzaro.; H. Pabst.; T. Müller.; R. Schade.; M. Guidon.; S. Andermatt.; N. Holmberg.; G. K. Schenter.; A. Hehn., A. Bussy.; F. Belleflamme.; G. Tabacchi.; A. Glöß.; M. Lass.; I. Bethune.; C. J. Mundy.; C. Plessl.; M. Watkins.; J. V. Vondele.; M. Krack.; J. Hutter. CP2K: An electronic structure and

molecular dynamics software package - Quickstep: Efficient and accurate electronic structure calculations. *J. Chem. Phys.* **2020**, *152*, 194103.
[S2] J. P. Perdew; K. Burke; M. Ernzerhof. Generalized Gradient Approximation Made Simple. *Phys. Rev. Lett.* **1996**, *77*, 3865-3868.
[S3] J. P. Perdew; K. Burke; M. Ernzerhof; Generalized Gradient Approximation Made Simple. *Phys. Rev. Lett.* **1997**, *78*, 1396-1396.
[S4] S. Grimme; J. Antony; S. Ehrlich; H. Krieg; A consistent and accurate ab initio parametrization of density functional dispersion correction (DFT-D) for the 94 elements H-Pu. *J. Chem. Phys.* **2010**, *132*, 154104.
[S5] S. Grimme; S. Ehrlich; L. Goerigk; Effect of the damping function in dispersion corrected density functional theory. *J. Comput. Chem.* **2011**, *32*, 1456-1465.
[S6] F. Weigend; R. Ahlrichs; Balanced basis sets of split valence, triple zeta valence and quadruple zeta valence quality for H to Rn: Design and assessment of accuracy. *Phys. Chem. Chem. Phys.* **2005**, *7* , 3297-3305.
[S7] F. Neese; The ORCA program system. *WIREs Comput. Mol. Sci.* **2012**, *2*, 73-78.
[S8] F. Neese; Software update: the ORCA program system, version 4.0. *WIREs Comput. Mol. Sci.* **2018**, *8*, e1327.
[S9] C. Adamo; V. Barone; Toward reliable density functional methods without adjustable parameters: The PBE0 model. J. Chem. Phys. **1999**, *110*, 6158-6170.
[S10] F. Weigend; Accurate Coulomb-fitting basis sets for H to Rn. *Phys. Chem. Chem. Phys.* **2006**, *8*, 1057-1065.
[S11] T. Lu; F. Chen; Multiwfn: A multifunctional wavefunction analyzer. J. Comput. Chem. **2012**, *33*, 580-592.

1.6 Cu_{58} catalyzed [3+2] azide-alkyne cycloaddition (AAC, click reaction).

Details of the catalytic procedure: 0.22 mmol phenylacetylene, 0.2 mmol benzyl azide and 3 mg Cu_{58} nanoclusters were added to a 10ml Shrek tube, 4ml acetonitrile was added as a solvent, the Shrek tube was vacuumed, and the reaction was carried out at 40 °C for 12 hours. The solvent containing the product can be obtained by filtration through the filter head, the product is determined as the target product by NMR hydrogen spectroscopy, and the yield is determined by gas chromatography to be 100%.

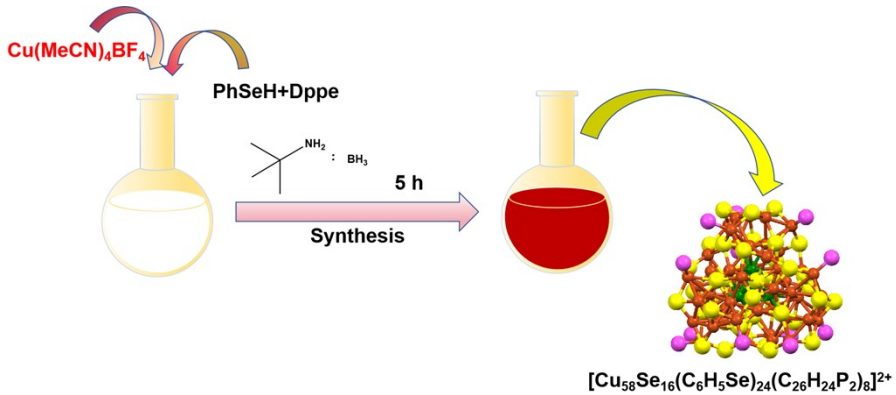

Figure S1. Synthesis of the $[Cu_{58}(SeC_6H_5)_{24}(Dppe)_6Se_{16}]^{2+}$ nanocluster.

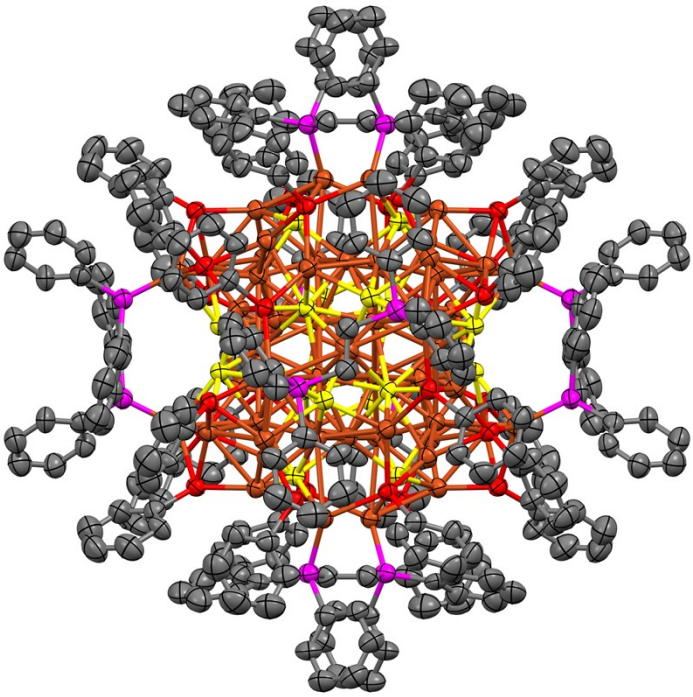

Figure S2. The ORTEP drawing (50% probability) of $[Cu_{58}(SeC_6H_5)_{24}(Dppe)_6Se_{16}]^{2+}$. Atom colours: Cu = brown, Se^{2-} = yellow, $Se_{(-C6H5)}$= Red, P = purple, C = grey. H atoms are omitted.

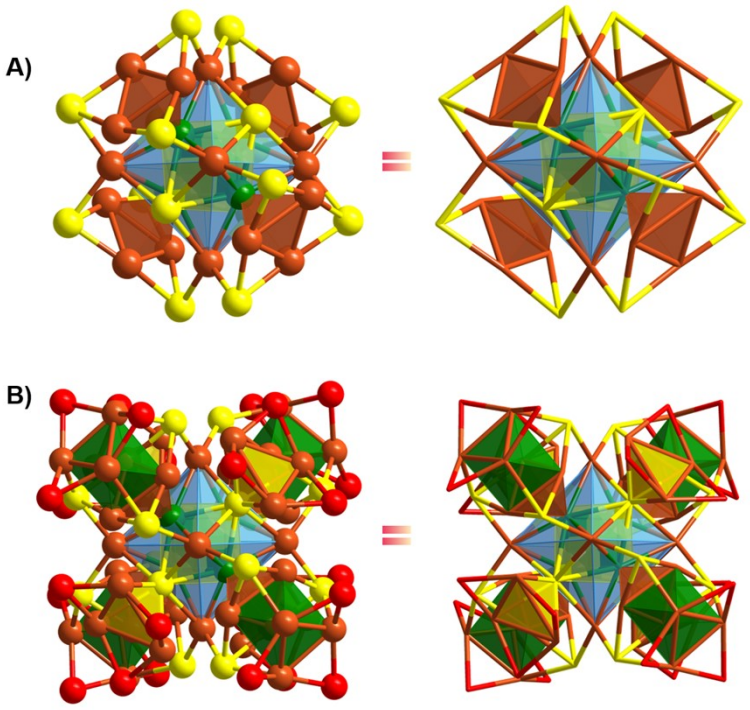

Figure S3. A) The framework structure of $Cu_4@Se_4@Cu_6$ core with four Cu_3Se_3 staples; B) The framework structure of $Cu_4@Se_4@Cu_6$ $@Cu_{12}Se_{12}$ with eight $Cu_3(SeR)_3$ staples. Atom colours: Cu = brown, Se^{2-} = yellow, $Se_{(-C6H5)}$= Red.

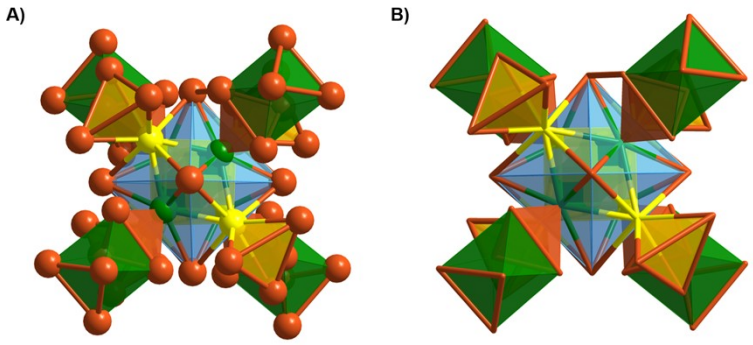

Figure S4. The $Cu_4@Se_4@Cu_6@Cu_{12}@Cu_{24}$ framework: an assembly of a series of tetrahedral units (Cu_4, Se_4 and Cu_3Se) and octahedral units (Cu_6). Atom colours: Cu = brown, Se^{2-} = yellow.

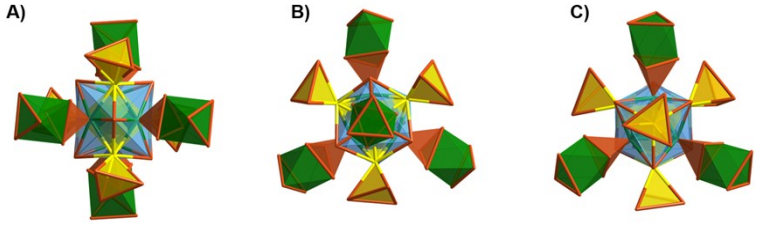

Figure S5. The $Cu_4@Se_4@Cu_6@Cu_{12}@Cu_{24}$ framework exhibits a C_2 or C_3 symmetry from different views. Atom colours: Cu = brown, Se^{2-} = yellow.

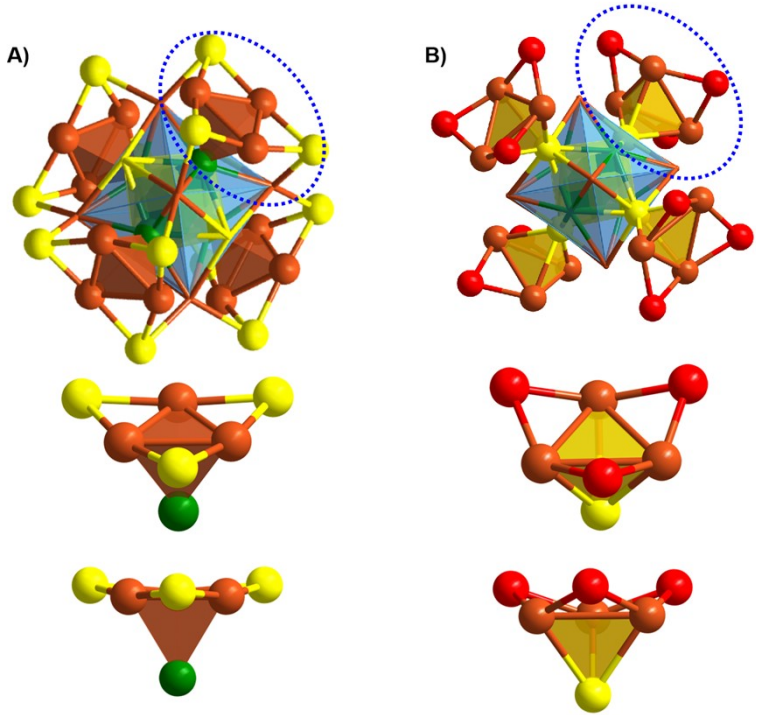

Figure S6. the structure of A) Cu_3Se_3 and B) $Cu_3(SeR)_3$. The atoms in Cu_3Se_3 are essentially coplanar, whereas the Se and Cu atoms in $Cu_3(SeR)_3$ reside in different planes. Atom colours: Cu = brown, Se^{2-} = yellow, $Se_{(-C6H5)}$= Red.

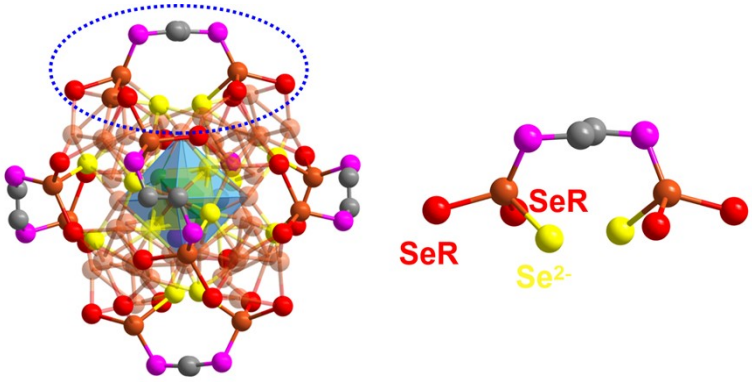

Figure S7. the bonding mode of $DppeCu_2$ units with the $Cu_4@Se_4@Cu_6@Cu_{12}Se_{12}@Cu_{24}(SeR)_{24}$. Six $DppeCu_2$ units encapsulate the surface of the framework by bonding each copper atom to two SeR groups and Se atoms. Atom colours: Cu = brown, Se^{2-} = yellow, $Se_{(-C6H5)}$= Red, P = purple, C = grey. H atoms are omitted.

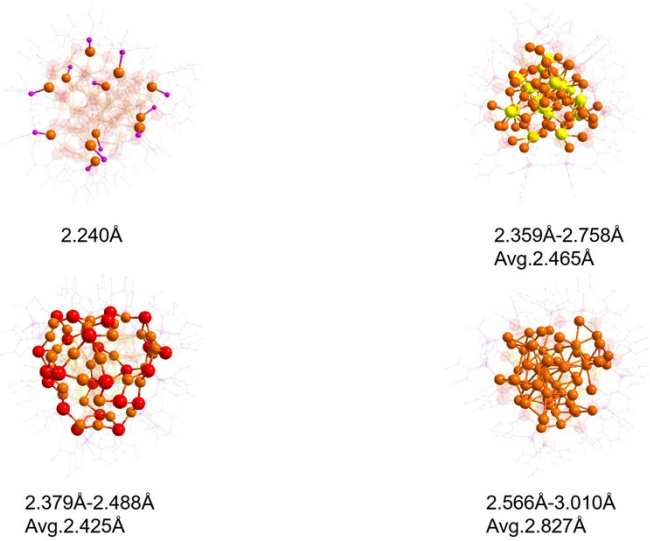

Figure S8. The Bond lengths of Cu_{58} nanoclusters. Atom colours: Cu = brown, Se^{2-} = yellow, Se(-C_6H_5)= Red, P = purple, C = grey.

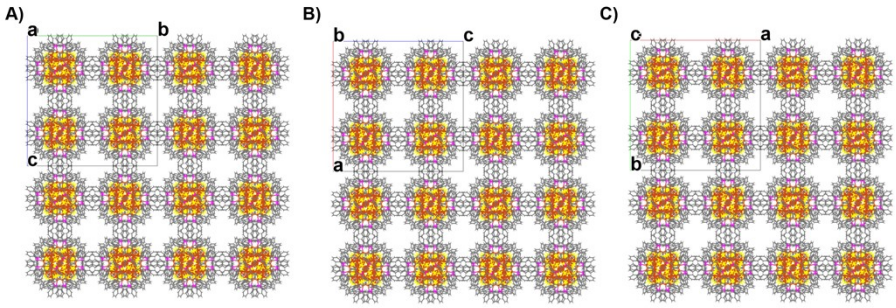

Figure S9. The packing mode of $[Cu_{58}(SeC_6H_5)_{24}(Dppe)_6Se_{16}]^{2+}$ from different views.

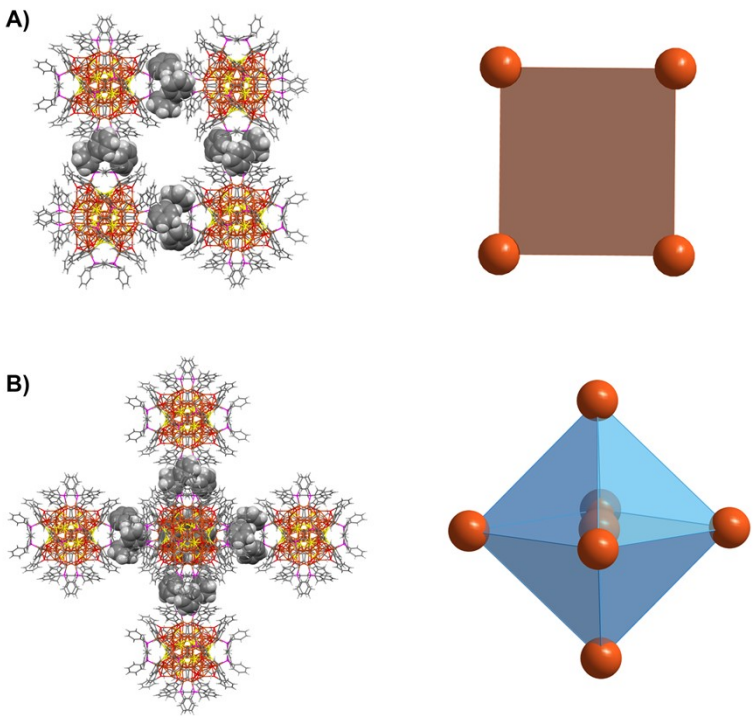

Figure S10. A) The bonding arrangement of four $[Cu_{58}(SeC_6H_5)_{24}(Dppe)_6Se_{16}]^{2+}$ in the same plane and B) the bonding arrangement of each cluster $[Cu_{58}(SeC_6H_5)_{24}(Dppe)_6Se_{16}]^{2+}$ with six surrounding clusters in three-dimensional structure. This precise packing pattern is driven by the interwoven interactions between the phenyl rings of face-to-face Dppe ligands and the inherent geometric compatibility of the structure.

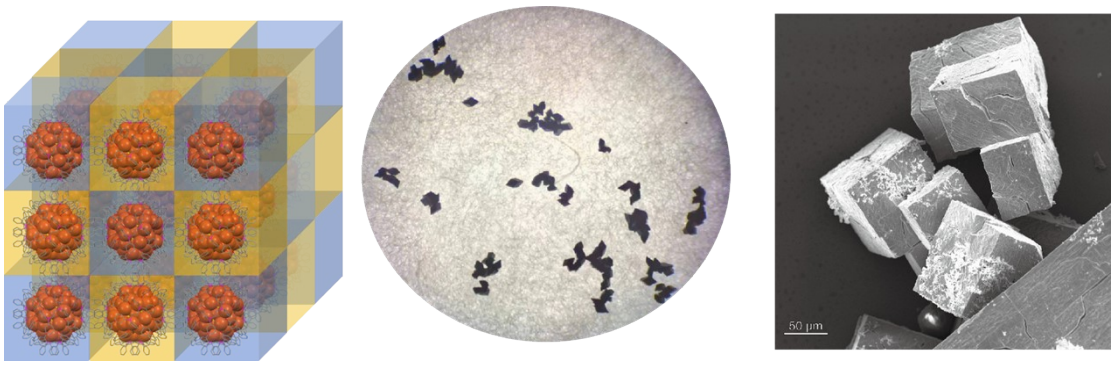

Figure S11. The highly ordered three-dimensional (3D) superlattice composed of individual clusters.

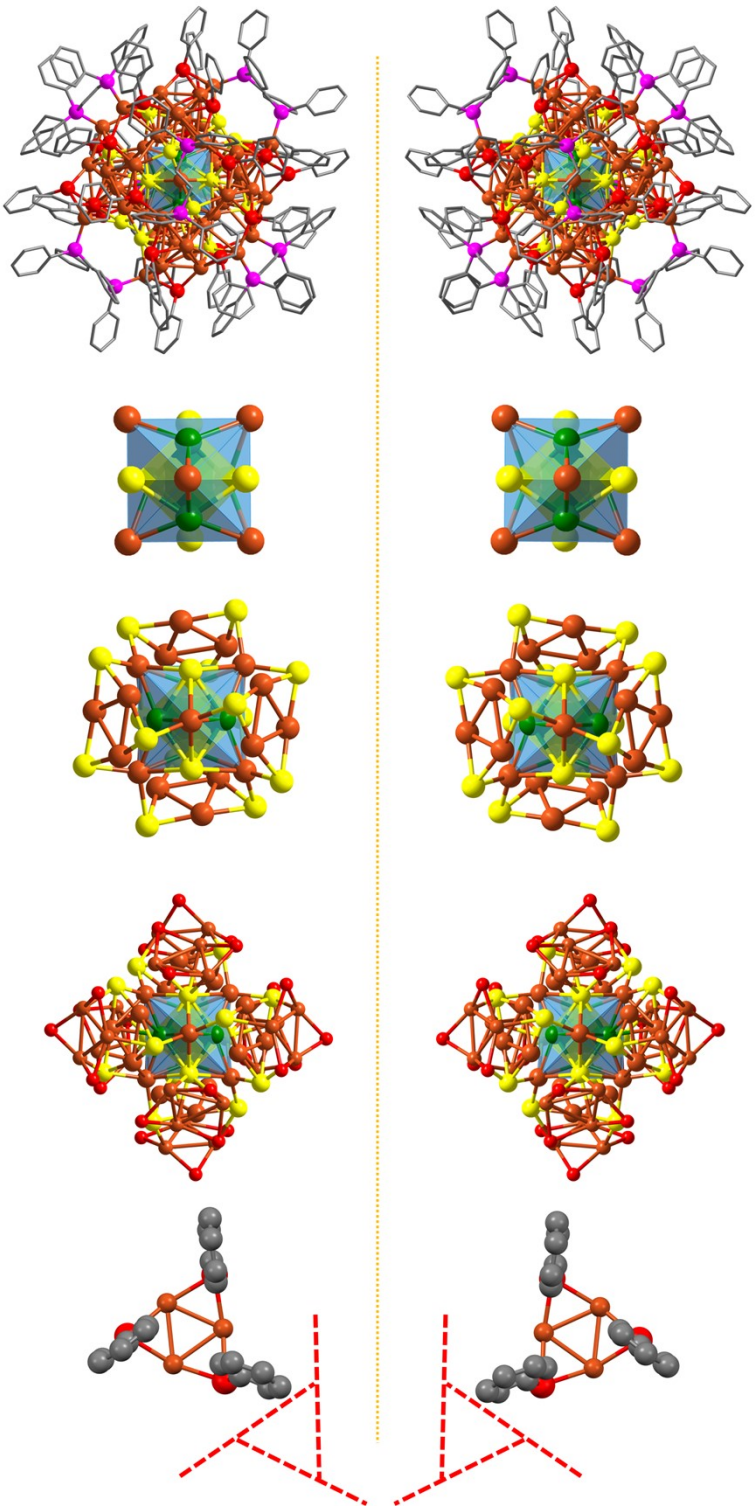

Figure S12. The structure of enantiomers. Detailed analysis reveals that the chirality arises from the asymmetrical arrangement of peripheral motifs and the core, as well as from the uneven distribution of ligands, which was further revealed by the following ECD spectra. Atom colours: Cu = brown, Se^{2-} = yellow, $Se_{(-C6H5)}$= Red, P = purple, C = grey. H atoms are omitted.

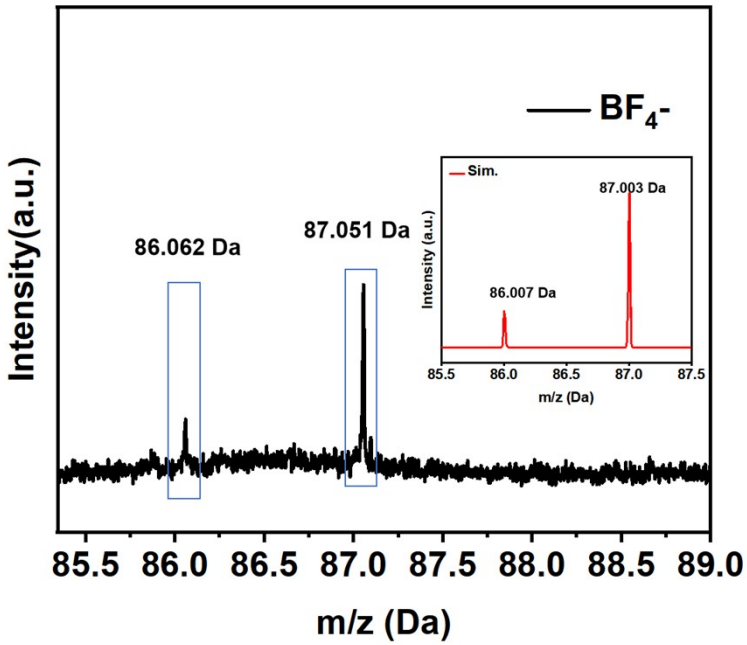

Figure S13. ESI-MS result of the BF_4^- counterion in $[Cu_{58}(SeC_6H_5)_{24}(Dppe)_6Se_{16}]^{2+}$ in negative mode. This suggests that the $Cu_{58}(SeC_6H_5)_{24}(Dppe)_6Se_{16}$ contains counter ions BF_4^-, although BF_4^- was not observed in the crystal structure.

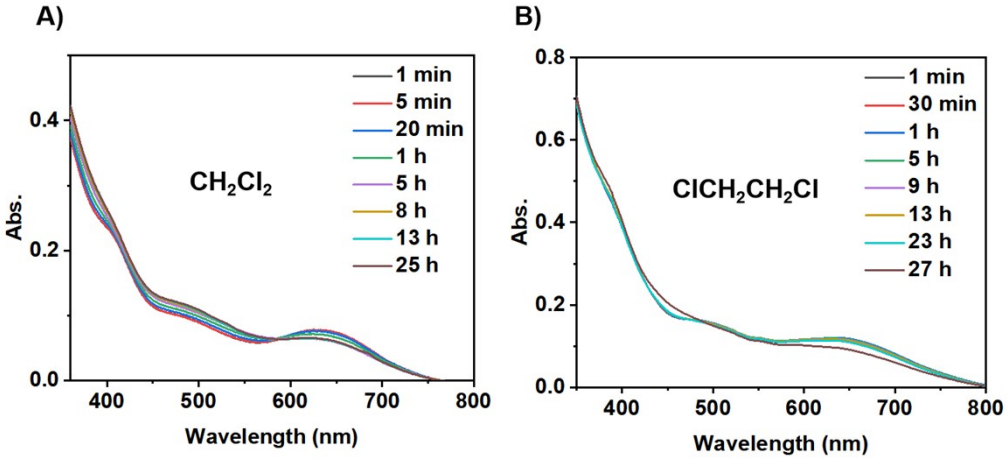

Figure S14. Stability test of $[Cu_{58}(SeC_6H_5)_{24}(Dppe)_6Se_{16}]^{2+}$ nanoclusters dissolved in A) CH_2Cl_2 and B) $ClCH_2CH_2Cl$ at room temperature. The solubility of $[Cu_{58}(SeC_6H_5)_{24}(Dppe)_6Se_{16}]^{2+}$ clusters was tested in various solvents including toluene, CH_2Cl_2, $CHCl_3$, CH_3OH, CH_3CH_2OH, CH_3CN, DMF, DMSO, and $ClCH_2CH_2Cl$. The clusters were practically insoluble in toluene, CH_3OH, CH_3CH_2OH, and CH_3CN, but showed good solubility in CH_2Cl_2, $CHCl_3$, DMF, DMSO, and $ClCH_2CH_2Cl$. However, $[Cu_{58}(SeC_6H5)_{24}(Dppe)_6Se_{16}]^{2+}$ decomposed easily in $CHCl_3$, DMSO and DMF solutions. In 1,2-dichloroethane, it demonstrated slightly better stability than in dichloromethane, remaining stable for over 25 hours.

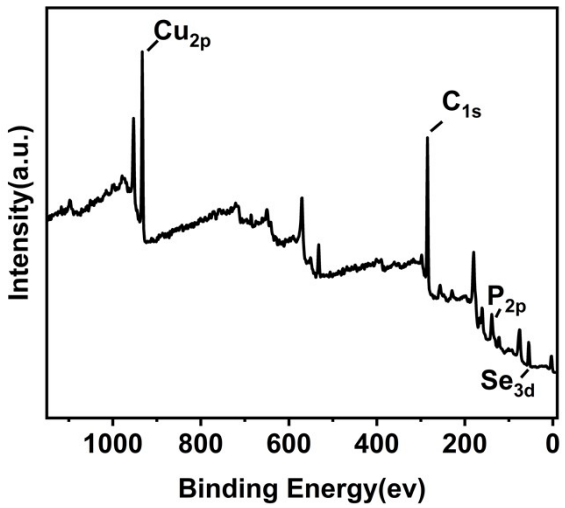

Figure S15. X-ray photoelectron spectroscopy (XPS) data for $[Cu_{58}(SeC_6H_5)_{24}(Dppe)_6Se_{16}]^{2+}$.

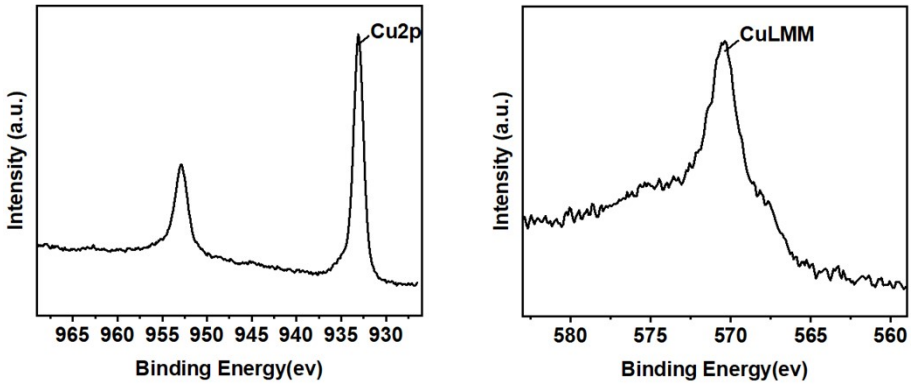

Figure S16. the XPS data of Cu2p and the Cu LMM spectra for $[Cu_{58}(SeC_6H_5)_{24}(Dppe)_6Se_{16}]^{2+}$.

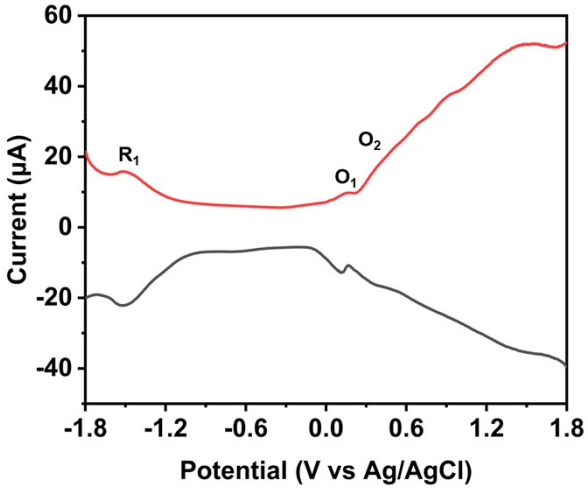

Figure S17. DPV of 0.015 mM $[Cu_{58}(SeC_6H_5)_{24}(Dppe)_6Se_{16}]^{2+}$ in CH_2Cl_2 with 0.1M TBAP. Pt disk was used as working electrode, Pt foil and Ag/AgCl were used as counterand reference electrode, respectively.

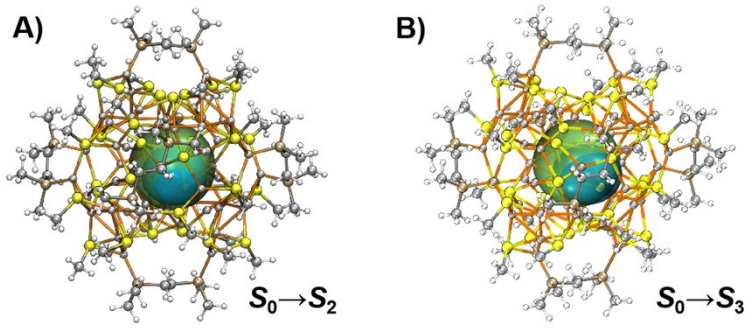

Figure S18. Three-dimensional contour maps of C_{hole} and C_{ele} functions of S_2 (A) and S_3 (B), which smoothly describe the distribution of hole and electron, respectively. Blue and green indicate holes and electrons, respectively.

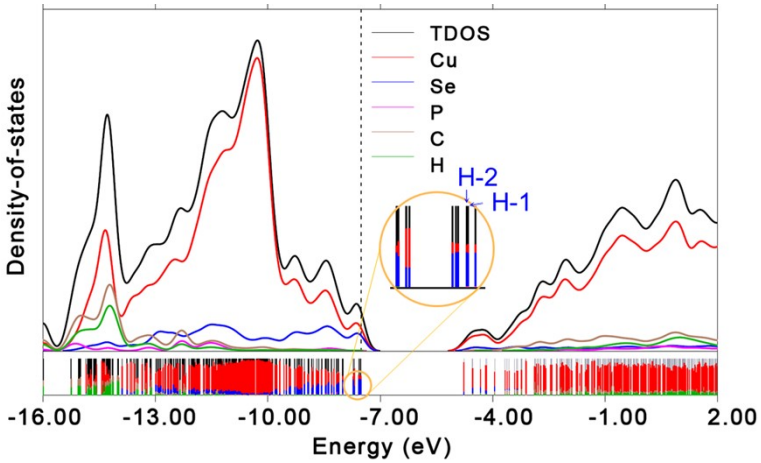

Figure S19. Calculated PDOS for **Cu_{58}**. Here the orbital energy range is set from -16 eV to 2 eV.

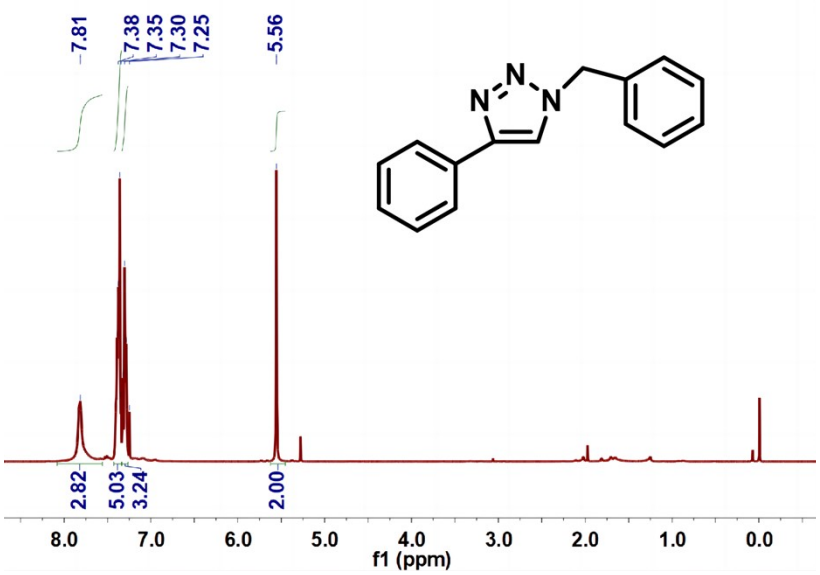

Figure S20. HNMR spectra of the product of phenylacetylene and benzyl azide at 40 °C as the model reaction.

Table S1. Crystal data and structure refinement for Cu_{58}.

Identification code	Cu_{58}
Empirical formula	$C_{300}H_{264}Cu_{58}P_{12}Se_{40}$
Formula weight	11084.91
Temperature/K	120(2)
Crystal system	cubic
Space group	F-43c
a/Å	46.782(3)
b/Å	46.782(3)
c/Å	46.782(3)
α/°	90
β/°	90
γ/°	90
Volume/Å^3	102383(18)
Z	8
ρ_{calc}g/cm^3	1.438
Crystal size/mm^3	0.1 × 0.1 × 0.08
Radiation	CuKα (λ = 1.54186)
2θ range for data collection/°	6.546 to 140.02
Index ranges	-41 ≤ h ≤ 55, -53 ≤ k ≤ 56, -54 ≤ l ≤ 56
Reflections collected	215151
Independent reflections	7639 [R_{int} = 0.0767, R_{sigma} = 0.0210]
Data/restraints/parameters	7639/150/261
Goodness-of-fit on F^2	1.068
Final R indexes [I>=2σ (I)]	R_1 = 0.0381, wR_2 = 0.0939
Final R indexes [all data]	R_1 = 0.0450, wR_2 = 0.0998
Largest diff. peak/hole / e Å^{-3}	0.43/-0.50

Table S2. The attribution of the theoretically simulated UV-Vis absorption peaks of **Cu_{58}**. Excited states with oscillator intensities less than 0.01 are ignored.

peak	Excited state (Sn)	Excited state Contribution(%)	Oscillator Strength	Transition mode	Transition contribution
α	1	22.649	0.0168	H→L	84.80%
	2	26.855	0.0188	H-1→L	42.60%
				H-2→L	40.30%
	3	21.157	0.0147	H-2→L	42.60%
				H-1→L	38.20%
β	98	12.95	0.0345	H→L+8	41.70%
	104	12.347	0.0332	H-1→L+8	33.70%

	101	5.344	0.0142	H-2→L+8	34.50%
				H-1→L+8	12.20%
	109	5.158	0.0145	H-4→L+8	36.90%
				H-3→L+8	10.70%
	100	4.637	0.0123	H-22→L	21.30%
				H-19→L	11.40%
	99	3.794	0.0101	H-1→L+8	13.00%
				H→L+8	7.40%
				H-14→L+1	6.90%
				H-21→L	6.20%
				H-13→L+2	6.20%
	83	3.63	0.0164	H-13→L+2	29.90%
				H-11→L+2	8.30%
	80	3.194	0.0163	H-11→L+3	37.90%
				H-3→L+7	5.90%
	77	2.357	0.0142	H-11→L+1	10.70%
				H-4→L+7	6.70%
				H→L+8	5.20%
γ	283	4.087	0.0249	H-16→L+6	11.30%
				H-37→L+3	5.40%
	293	3.806	0.0214	H-3→L+12	7.90%
				H-2→L+12	5.60%
				H-38→L+2	5.60%
	318	2.543	0.0172	H→L+13	11.90%
				H-42→L+2	8.00%
				H-10→L+11	5.60%
	291	2.248	0.0127	H-9→L+9	8.50%
				H-13→L+8	8.20%
				H-8→L+10	7.10%
				H-38→L+1	6.70%
	329	2.11	0.0168	H-41→L+3	5.10%
				H-10→L+10	5.10%
	275	2.072	0.0134	H-6→L+10	6.40%
	292	2.005	0.0113	H-3→L+12	9.90%
				H→L+12	7.40%
				H-39→L+3	6.00%
	307	1.998	0.0119	H-9→L+9	12.90%
				H-4→L+12	8.20%
	278	1.928	0.0122	H-46→L	5.90%